

Sensitivity to grain discretization of the simulated crystal stress distributions in FCC polycrystals

H Ritz and P R Dawson

Mechanical and Aerospace Engineering, Cornell University, Ithaca, NY 14853, USA

E-mail: hr32@cornell.edu

Received 13 June 2008, in final form 29 September 2008

Published 5 November 2008

Online at stacks.iop.org/MSMSE/17/015001

Abstract

An elastoviscoplastic finite element model of aluminum alloys is used to compare mechanical response among meshes formed with several different grain shapes. Tetrahedral elements are used to form grains of cubic, rhombic dodecahedral and truncated octahedral shape. The influence of the grain shape on the aggregate response is examined in terms of the stress variation and the aggregate elastic moduli. While elastic anisotropy in the bulk material is not found to be dependent on grain shape, consistent trends are observed in intragranular and intergranular stress distributions across these mesh definitions.

1. Introduction

Polycrystalline metals constitute an important class of engineering materials, and accurately predicting their response to mechanical manipulation and loading allows increased efficiency in their forming and utilization. Modelling on the polycrystal, or aggregate, level gives insight into material behaviors such as orientational texture evolution and formation of residual stresses. Here, an aggregate is a group of crystals that act collectively to define the bulk behavior. Of particular interest is how the properties of the constituent crystals are expressed in the behavior of the bulk. Confidence in a model enables the determination of aggregate properties from crystal properties or vice versa. A major issue in this regard is whether a model accurately captures the grain (crystal) interactions, including their dependencies on the grain morphology and topology, as these interactions are the physical link between crystals acting individually and aggregates of crystals acting collectively. 'Grain interactions' generally refers to the ways in which neighboring grains affect each other's stress development and reorientation during the course of deformation of the bulk.

All models have target applications and assessing the fidelity of a model involves determining its accuracy within that scope. The targeted behavior of the finite element (FE) model considered here is the elastoplastic response of polycrystalline materials under

mechanical loading at moderate strain rates. In assessing a model it is necessary to examine its construct in several respects; governing equations, methodologies invoked to obtain solutions, and robustness to variations of input data are the main components. For polycrystals, the rendering of an aggregate is also important. Variables available for this task include the number of degrees of freedom within each crystal, the morphology (shape) of the crystals and the topology associated with their arrangement. These simple variables can have an impact on bulk behavior. For example, Bunge *et al* [1] explored the effects of grain shape and packing on the elastic properties of polycrystals, using grains of three different shapes to do so. They found that the influence of these factors can be up to 25% of the total texture influence. The influence of these geometric properties of the grains on the fidelity of the simulation results, particularly the stresses within crystals, is the focus of the current paper.

For polycrystals, grain interactions occur via intergranular tractions. These intergranular tractions are the local boundary conditions for grains and thus control the stress internal to the grains. The stress observed at the macroscopic scale may be computed from averaging over an external surface of an aggregate. To fully assess a model it is necessary to compare model results with experimental results not only through this aggregate average but also through the distribution of crystal stresses within the aggregate, assuming that a goal of the model is to illuminate how crystals act collectively. Since the created domain can never be completely naturalistic it is possible that some aspect of the virtual samples may introduce an aphysical artefact. By insisting on assessment of the accuracy at the crystal level as well as for the aggregate average to determine that any artefacts are at an acceptably small level (and lacking a mathematical proof), it is necessary to have measurements of the response at the scale of crystals as a basis for comparison.

Diffraction (x-ray or neutron) provides lattice spacing data. Using changes in the spacing during *in situ* mechanical loading, individual components of the lattice (elastic) strain can be determined. The crystal stress may be evaluated directly from the strain using Hooke's law, provided the strain tensor is completely determined and the single crystal properties are well known. Lattice strains can be measured within a single grain via micro-diffraction or for sets of crystals corresponding to a particular crystallographic fiber via bulk diffraction. From these data, it is possible to quantify, for example, the elastic anisotropy via directional diffraction elastic moduli, and the variability of strain, either between grains of different orientation (using bulk diffraction) or within small sets of grains (using micro-diffraction). Since these behaviors reflect the influences abutting crystals can have on each other, an accurate simulation with physically sound accounting of grain interactions should be able to capture what is observed, both qualitatively and quantitatively. These behaviors, therefore, give us a basis for critiquing the model performance. In the past there has been incomplete success in predicting the degree of elastic anisotropy that manifests during deformation [2, 3]. The FE simulations tend to show less difference in lattice strains between crystals with different orientations relative to the experiments. Part of that discrepancy can be attributed to physical changes in the single crystal material properties upon alloying [4, 5], but that does not completely account for the difference. Knowing the extent to which the grain and bulk instantiation (i.e. formation of the FE representation of the physical specimen) itself influences the results may shed further light on this discrepancy and is necessary before the simulations can be used with confidence either to predict aggregate behaviors from that of single crystals or to infer single crystal properties from aggregate averages.

In this paper we will begin by describing the modelling framework, both in terms of the model equations and in terms of specimen instantiation. We will further discuss those aspects of the diffraction experiments relevant to comparing simulation results with experimental data, including a thorough description of how these particular simulations have been tied

to experiments. We then present the simulation results, focussing on the diffraction moduli and the spatial variability of stress as the methods of investigating the effects of different grain discretizations. Finally, we conclude with the implications of these results on future modelling endeavours.

2. Virtual polycrystals

The simulations used in this study are performed using a parallel computational implementation of an elastoviscoplastic FE formulation. The large scale parallel nature of the simulations gives us the ability to have many degrees of freedom within each crystal in the bulk material while still following a volume large enough to accurately portray statistical trends. In this way it is possible to examine the essential focus of this study, the way strains and stresses develop in different grains.

When modelling polycrystalline material deformation there are several scales to consider, including most notably the scale of the bulk volume and the scale of the grains. In such models as we employ here the scale of dislocation motion is not considered; material deformation is assumed to take place through dislocation motion along slip planes, but the details are replaced by discrete slip modes. Properties and values quantifiable on the bulk scale include macroscopic specimen strain, macroscopic stress and bulk elastic properties such as average Young's modulus and Poisson's ratio. Similar quantities are defined on the crystal scale, including lattice strains, anisotropic single crystal elastic moduli, crystal stresses and lattice orientation.

In this section we first describe the model equations and formulation used and then discuss instantiation of the specimens into the simulation framework using grains with different shapes and packing arrangements.

2.1. Mechanical response of virtual specimens

An elastoviscoplastic FE formulation was used to simulate the response of the specimens to a loading history of uniaxial tension. This FE formulation has the benefit of *a priori* satisfying compatibility everywhere like other displacement or velocity-based formulations through the use of continuous trial functions for the velocity. The equilibrium equations are satisfied in a weak sense. The deformation is assumed to be quasi-static; that is, the effects of momentum are small and can be neglected. The weak form of the equilibrium equations may be written as:

$$R_u = - \int_B \text{tr}(\boldsymbol{\sigma}'^T \text{grad} \boldsymbol{\psi}) dB + \int_B \pi \text{div} \boldsymbol{\psi} dB + \int_{\Gamma} \boldsymbol{t} \cdot \boldsymbol{\psi} d\Gamma + \int_B \boldsymbol{\iota} \cdot \boldsymbol{\psi} dB, \quad (1)$$

where R_u is the residual to be minimized, $\boldsymbol{\psi}$ are vector weighting functions, \boldsymbol{t} is the traction vector, $\boldsymbol{\iota}$ is a body force per unit volume, B is the volume of the body and Γ is its surface¹. The deviatoric Cauchy stress, $\boldsymbol{\sigma}'$, and mean stress (negative of the pressure, π) sum to the total Cauchy stress: $\boldsymbol{\sigma} = \boldsymbol{\sigma}' - \pi \boldsymbol{I}$. Traction or velocity is specified over the boundary.

The stress is replaced ultimately with the velocity field through introduction of the constitutive equations and the kinematic relation defining the velocity gradient. Equations for the elastic and plastic responses are required to model the regimes of behavior that exist in the tests. For the elastic behavior we use Hooke's Law for cubic symmetry. For the plastic behavior, we assume restricted slip along the close-packed planes and in the close-packed

¹ Throughout this paper, boldface quantities denote vectors and tensors; scalars and components of vectors and tensors are written using a normal weight font. Subscripts appear as descriptive labels for scalars or tensor components; there is no use of indicial notation.

directions. The elastic and plastic behaviors are combined through a kinematic decomposition of the total deformation gradient, \mathbf{f} , by the following three-part multiplicative decomposition:

$$\mathbf{f} = \mathbf{f}^b \mathbf{f}^* \mathbf{f}^\# = \mathbf{v}^b \mathbf{r}^* \mathbf{f}^\# \quad (2)$$

Here $\mathbf{f}^\#$ is the purely plastic part of \mathbf{f} arising from slip, \mathbf{f}^* is the lattice rotation which may be written as \mathbf{r}^* and \mathbf{f}^b is the elastic part of \mathbf{f} . The deformation gradient $\mathbf{f}^\#$ can be used to define an intermediate configuration, $\hat{\mathcal{B}}$, which is a relaxed configuration obtained by unloading without rotation from the current configuration \mathcal{B} . Using this interpretation of $\hat{\mathcal{B}}$, the symmetric left elastic stretch tensor, \mathbf{v}^b , is introduced. For the case of small elastic strains (\mathbf{e}^b), $\mathbf{v}^b = \mathbf{I} + \mathbf{e}^b$, where $\|\mathbf{e}^b\| \ll 1$ and \mathbf{I} is the second order identity tensor.

The velocity gradient, $\mathbf{I} (\equiv \partial \mathbf{u} / \partial \mathbf{x})$, where \mathbf{u} is the velocity and \mathbf{x} are the current coordinates), is obtained by differentiation of the deformation gradient with time and is split into the deformation rate tensor, $\mathbf{d} \equiv \text{sym}(\mathbf{I})$, and the spin tensor, $\mathbf{w} \equiv \text{skw}(\mathbf{I})$, expressed in the current configuration \mathcal{B} . These terms may be split further into spherical and deviatoric parts to give:

$$\begin{aligned} \text{tr}(\mathbf{d}) &= \text{tr}(\dot{\mathbf{e}}^b), \\ \mathbf{d}' &= \dot{\mathbf{e}}^{b'} + \hat{\mathbf{d}}^{\#'} + \mathbf{e}^{b'} \hat{\mathbf{w}}^\# - \hat{\mathbf{w}}^\# \mathbf{e}^{b'}, \\ \mathbf{w} &= \hat{\mathbf{w}}^\# + \mathbf{e}^{b'} \hat{\mathbf{d}}^{\#'} - \hat{\mathbf{d}}^{\#'} \mathbf{e}^{b'}, \end{aligned} \quad (3)$$

where a prime (\cdot') indicates the deviatoric component of a quantity and the ($\hat{\cdot}$) superscript indicates mapping forward by \mathbf{r}^* according to

$$\hat{\mathbf{w}}^\# = \mathbf{r}^* \mathbf{w}^\# \mathbf{r}^{*\text{T}} \quad \text{and} \quad \hat{\mathbf{d}}^{\#'} = \mathbf{r}^* \mathbf{d}^{\#'} \mathbf{r}^{*\text{T}} \quad (4)$$

to define the plastic deformation rate tensor, $\hat{\mathbf{d}}^{\#'}$, and the plastic spin tensor, $\hat{\mathbf{w}}^\#$, in the relaxed configuration $\hat{\mathcal{B}}$ (both $\mathbf{w}^\#$ and $\mathbf{d}^{\#'}$ are defined relative to $\mathbf{f}^\#$).

Equations for the elastic and plastic responses are introduced into the kinematic decomposition given by equation (3). The elastic response follows a linear relation:

$$\boldsymbol{\tau} = \mathbb{C} \mathbf{e}^b \quad \text{with} \quad \mathbb{C} = \mathbb{C}(\mathbf{r}), \quad (5)$$

where \mathbb{C} is the tensor containing elastic moduli for cubic crystal symmetry, which depends on the orientation of the crystallographic lattice, \mathbf{r} . The Kirchhoff stress, $\boldsymbol{\tau}$, is related to the Cauchy stress, $\boldsymbol{\sigma}$, through $\boldsymbol{\tau} = \beta \boldsymbol{\sigma}$, where $\beta = \det(\mathbf{v}^b)$.

The viscoplastic flow rule is derived from the crystallographic slip and is defined as:

$$\hat{\mathbf{I}}^\# = \hat{\mathbf{d}}^{\#'} + \hat{\mathbf{w}}^\# = \dot{\mathbf{r}}^* \mathbf{r}^{*\text{T}} + \sum_{\alpha} \dot{\gamma}^{\alpha} (\hat{\mathbf{T}}^{\alpha}), \quad (6)$$

where $\hat{\mathbf{T}}^{\alpha}$ is the Schmid tensor, $\hat{\mathbf{T}}^{\alpha} = \mathbf{b}^{\alpha} \times \mathbf{m}^{\alpha}$, and \mathbf{b}^{α} and \mathbf{m}^{α} are the slip direction and the slip plane normal for the α -slip system in configuration $\hat{\mathcal{B}}$. The assumed slip systems for the FCC crystals are the 12 systems with $\langle 110 \rangle$ directions and $\{111\}$ normals. Using these relations, the symmetric and skew symmetric parts of the plastic velocity gradient, $\hat{\mathbf{d}}^{\#'}$ and $\hat{\mathbf{w}}^\#$, respectively, are defined as:

$$\hat{\mathbf{d}}^{\#'} = \sum_{\alpha} \dot{\gamma}^{\alpha} \hat{\mathbf{P}}^{\alpha} \quad \text{and} \quad \hat{\mathbf{w}}^\# = \dot{\mathbf{r}}^* \mathbf{r}^{*\text{T}} + \sum_{\alpha} \dot{\gamma}^{\alpha} \hat{\mathbf{Q}}^{\alpha}, \quad (7)$$

where

$$\hat{\mathbf{P}}^{\alpha} = \hat{\mathbf{P}}^{\alpha}(\mathbf{r}) = \text{sym}(\hat{\mathbf{T}}^{\alpha}) \quad \text{and} \quad \hat{\mathbf{Q}}^{\alpha} = \hat{\mathbf{Q}}^{\alpha}(\mathbf{r}) = \text{skw}(\hat{\mathbf{T}}^{\alpha}). \quad (8)$$

Using the symmetric portion of the Schmid tensor to define the stress active on the α -slip system, the plastic shearing rate, $\dot{\gamma}^\alpha$, is related to the resolved shear stress, τ^α , by a power law relation:

$$\dot{\gamma}^\alpha = \dot{\gamma}_0 \left(\frac{|\tau^\alpha|}{g^\alpha} \right)^{\frac{1}{m}} \text{sgn}(\tau^\alpha) \quad \text{with} \quad \tau^\alpha = \text{tr}(\hat{\mathbf{P}}^\alpha \boldsymbol{\tau}'), \quad (9)$$

where g^α is the slip system hardness, $\dot{\gamma}_0$ is a reference shear rate and m is the rate sensitivity of slip. With the help of a time differencing of the elastic strain rate, the equations for the elastic and plastic responses are merged in the rate form of the kinematic decomposition and used to eliminate the stress in the equilibrium residual. The residual is cast in discretized form through the introduction of piece-wise trial and weight functions to yield a matrix equation for the velocity field at the end of each time step.

To complete the solution methodology the lattice orientations, \mathbf{r} , and slip system strengths, g , must be advanced over time. The lattice orientation evolves as a consequence of the spin and is given by:

$$\dot{\mathbf{r}} = \frac{1}{2}\boldsymbol{\omega} + (\boldsymbol{\omega} \cdot \mathbf{r})\mathbf{r} + \boldsymbol{\omega} \times \mathbf{r} \quad \text{where} \quad \boldsymbol{\omega} = \text{vect} \left(\hat{\mathbf{w}}^\# - \sum_{\alpha} \dot{\gamma}^\alpha \hat{\mathbf{Q}}^\alpha \right). \quad (10)$$

Slip system strength (hardness) evolution is assumed to follow a Voce form, expressed as

$$\dot{g} = h_0 \left(\frac{g_s - g}{g_s - g_0} \right)^n \dot{\gamma} \quad \text{where} \quad \dot{\gamma} = \sum_{\alpha} |\dot{\gamma}^\alpha|. \quad (11)$$

The four material parameters in (11) are the initial slip system hardening rate, h_0 , the saturation slip system strength, g_s , the initial slip system strength, g_0 , and a hardening exponent, n . Each of these equations is numerically integrated in concert with the incremental solution for the motion. We discuss determination of these parameters in section 4.1.3.

2.2. Instantiation of virtual specimens

When dividing the FE domain into grains there are many choices including both regular tessellations using one shape congruently repeated throughout space and irregular tessellations using multiple (and not necessarily congruent) shapes to fill space. Using irregular tessellations it may be possible to generate a less idealized and more realistic array of grain shapes, but there are drawbacks. It often takes many more elements to represent a smaller number of grains. Also, since we wish to observe the influence of grain shape and organization on crystal stress distributions we choose to use only regular tessellations which have more easily quantifiable and homogeneous attributes throughout the mesh. There are a limited number of parallelohedra (polyhedra that fill space via parallel translations) in \mathbb{R}^3 [6]. These are cubes, hexagonal prisms, truncated octahedra, hexarhombic dodecahedra and rhombic dodecahedra. We chose cubes, truncated octahedra and rhombic dodecahedra, following the choices in [1], and created FE meshes of a unit cube with grains in each of those shapes. In all cases the elements are ten-noded tetrahedra and grains are formed by sharing a common initial crystal orientation between groups of these elements arranged in the correct shapes. Figure 1 shows a small number of grains from each of those meshes, and figure 2 shows the complete mesh of octahedral grains, both with and without the boundary grains, which demonstrates that incomplete grains are present at the boundaries of the mesh to build a smooth unit cube volume. Delannay *et al* studied the effects of grain discretization on texture evolution using both cubic and truncated octahedral grains, and found the octahedral grains to be more effective at matching experimental trends for texture evolution under plane strain compression [7]. In that study all elements were 8-noded

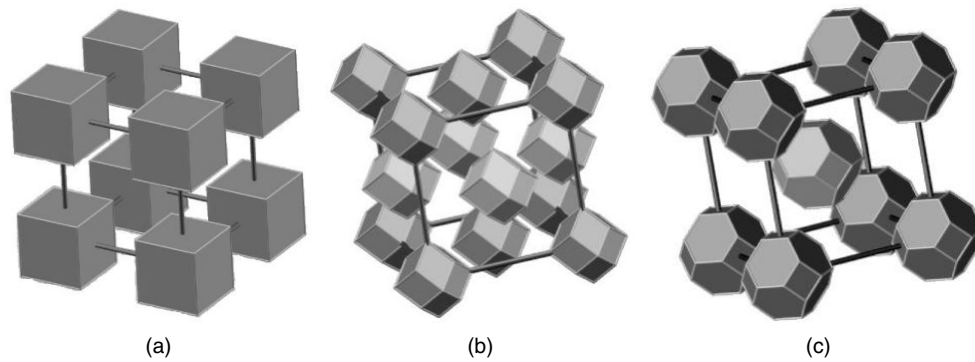


Figure 1. A small cluster of grains (showing the packing type) for (a) cubic, (b) dodecahedral and (c) truncated octahedral grains. The distance between the centroids of the grains has been increased to emphasize the grain shape and packing structure; the actual meshes are space-filling.

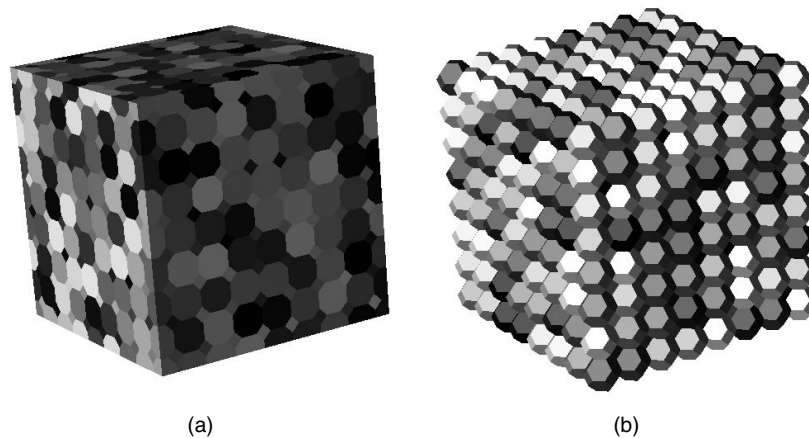


Figure 2. (a) Complete mesh composed of octahedral grains, filling a unit cube of volume exactly. (b) The same mesh with only the grains which have 72 elements, forming complete octahedra. All partial grains have been stripped away from the boundary. In both subfigures, all elements forming a single grain are given the same random shading to aid in visualizing the grains.

bricks, with 16 elements per octahedral grain and either one or 27 elements per cubic grain. Here we use higher order elements with more degrees of freedom in each type of grain and focus on stress distributions in the simulation results.

When a complete mesh is composed from each of the grain shapes, a unique packing structure results. If you consider the centroid of each grain to be a lattice point and compose unit cells based on the locations of these lattice points, cubic grains create unit cells equivalent to a simple cubic (SC) pattern. Similarly, dodecahedral grains lie on lattice points whose unit cell is equivalent to a face-centered cubic (FCC) lattice, and the octahedral grains form a body-centered cubic (BCC) unit cell. These patterns are illustrated in figure 1. Table 1 shows some interesting and relevant properties of the different grains. The attributes assumed to be of most importance are the number of nearest neighbors and the number of degrees of freedom per grain.

Table 1. Geometric properties of different grain shapes and the meshes composed from them. The ‘surface area per unit volume’ measurement assumes each grain has volume 1 [L^3] and the measurement itself is in units of [L].

	Cube	Rhombic dodecahedron	Truncated octahedron
Packing structure	SC	FCC	BCC
Vertices	8	14	24
Edges	12	24	36
Faces (nearest neighbors)	6	12	14
Surface area per unit volume	6.00	5.35	5.31
Elements per grain	24	48	72
Degrees of freedom per grain	195	303	550
Grains in mesh	3375	2360	1241

3. Observations from diffraction measurements of *in situ* mechanical loading

Confidence in models can always be improved by showing favourable comparisons with experiments. Conversely, the inability to reproduce observed behaviors exposes weaknesses or limitations of the model, its implementation, or its robustness. The type of experiments we use here are diffraction measurements on materials undergoing *in situ* uniaxial mechanical loading. These *in situ* diffraction experiments provide data of particular relevance to grain interactions, though some difficulties do arise. While much information is available on the macroscopic scale, including the overall stress and strain through knowledge of the applied load and initial cross section and through extensometer data, more limited information is available on the crystal scale. Lattice strains can be measured by means of diffraction, but the stresses cannot be measured directly in polycrystalline samples. A further complication arises in the neutron diffraction (ND) techniques employed here because the lattice strains are not measured in individual crystals but rather in groups of crystals sharing an axis of orientation, as described in section 3.1. Since some information is lacking on the crystal scale or is known only as an average over a crystallographic fiber, it is necessary to invoke modelling assumptions to bridge the scales to the data that is available [8]. Previous efforts to bridge these scales include Voigt’s isostrain (upper bound) [9], Reuss’s isostress (lower bound) [10] and the work of Kroner [11], who utilized Eshelby’s [12] self-consistent model to find the polycrystal elastic constants based on the anisotropic single crystal elastic constants. Bollenrath *et al* [13], Hayakawa *et al* [14], De Wit [15] and Gnaupel-Herold *et al* [16] have all extended Kroner’s work to incorporate elastic moduli measurable through diffraction.

In this section after briefly describing diffraction measurements in general, including both bulk diffraction and micro-diffraction, we describe the data in which we are interested from these experiments and the method of reducing them, focussing on those data that illuminate the importance of grain morphology and discretization.

3.1. Diffraction experiments

In situ diffraction experiments consist of macroscopically loading a specimen through a predetermined deformation path and performing diffraction measurements at various loads. Typically the macroscopic loading is uniaxial in nature and can be either tensile or compressive, though other types of loading are possible, such as high temperature and pressure [17, 18]; here we use uniaxial tension. The ND measurements themselves consist of lattice strains at certain macroscopic stress levels. Since these are uniaxial tension experiments, the macroscopic stress

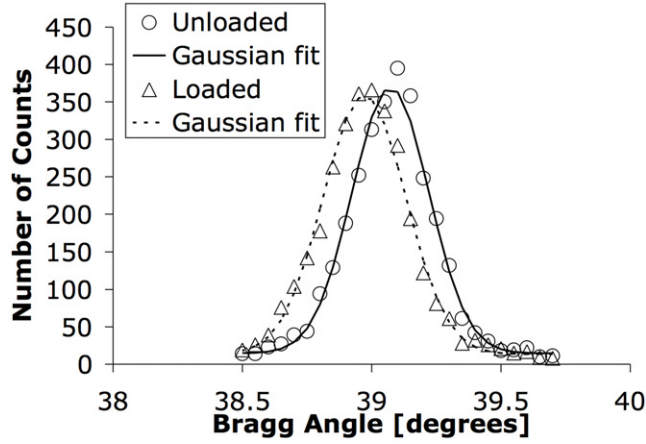


Figure 3. A typical measured diffraction peak, both unloaded and under load, along with Gaussian distributions fit to the data. The individual data points refer to the number of neutrons detected at the corresponding Bragg angle during a diffraction measurement.

value we use is simply the force applied, measured by a load cell, divided by the initial specimen cross-sectional area, measured before the test begins. The lattice strains are found by taking advantage of Bragg's law [19]:

$$n\lambda = 2\bar{d}_{hkl} \sin \bar{\theta}_{hkl}, \quad (12)$$

where n is an integer, λ is the wavelength of the incoming radiation, $\bar{\theta}_{hkl}$ is the diffraction angle and \bar{d}_{hkl} is the spacing between $\{hkl\}$ lattice planes. During a ND experiment for a particular $\langle hkl \rangle$, constructive interference consistent with Bragg's law occurs along a fiber in orientation space defined by

$$\mathbf{R}\mathbf{c} = \pm\mathbf{s}, \quad (13)$$

where \mathbf{R} is the orientation matrix of a crystal, \mathbf{c} is the crystallographic direction corresponding to the $\langle hkl \rangle^2$ currently under consideration and \mathbf{s} is the sample direction corresponding to the scattering vector, usually aligned either parallel or normal to the uniaxial tension axis. The diffraction measurements cannot distinguish between grain satisfying (13). Therefore, in diffraction of bulk specimens where the radiation beam covers a large volume of the specimen all $\bar{\theta}_{hkl}$ and \bar{d}_{hkl} measurements are averages over groups of crystals, including both crystals with identical orientations and crystals related by a simple rotation about the \mathbf{s} axis. Furthermore, there is a certain amount of experimental leeway in the alignment necessary between \mathbf{c} and \mathbf{s} to contribute to a measurement. Equation (13) need not be satisfied exactly, but an alignment between \mathbf{c} and \mathbf{s} within a small angular range (up to 5° for certain experiments) results in a contribution to the diffraction measurement. An example of a measured diffraction peak is shown in figure 3. The individual data points are counts from the detector at each specific angle. A Gaussian distribution is fit to the measured data, and the center of that peak is $\bar{\theta}_{hkl}$. The peak intensity is related to the multiplicity of the $\langle hkl \rangle$ under consideration and the length of time that the detector was counting and is not a factor for this study.

The measured spacing, \bar{d}_{hkl} , is compared with the reference spacing, \bar{d}_{hkl}^0 , (measured at a nominally zero load prior to any deformation) through (14) to determine the average normal

² In cubic crystals, such as we consider here, $\langle hkl \rangle$ is always the direction perpendicular to the $\{hkl\}$ planes, and we forgo use of the convention of uvw to denote directions.

component of lattice strain on $\{hkl\}$ planes in the s direction, $\epsilon_{(hkl)}^D$,

$$\epsilon_{(hkl)}^D = \frac{\bar{d}_{hkl} - \bar{d}_{hkl}^0}{\bar{d}_{hkl}^0}. \quad (14)$$

In addition to a shift in position, the diffraction peaks also experience a broadening and slight decrease in maximum intensity as the crystals are loaded and strained.

In contrast to bulk diffraction, the beam size in micro-diffraction experiments may be smaller than the size of an individual grain. In that case $\epsilon_{(hkl)}^D$ is not the result of averages among many grains, but can be measured on a crystal-by-crystal basis, or even at multiple locations within a single crystal [20, 21].

3.2. Elastic anisotropy

The lattice strains as measured by bulk ND experiments will in general show different levels of strain for different crystallographic fibers. This is partially due to elastic anisotropy in the single crystal but is also heavily influenced by crystallographic texture and the arrangement of grains and their neighbors. It is possible that grain morphology may affect the expression of elastic anisotropy. There are two manifestations of elastic anisotropy of concern in this study. The first is the single crystal elastic anisotropy and the second is the diffraction anisotropy, which is measured from a bulk polycrystal. If grain interactions (i.e. neighboring grains imparting tractions on each other, producing a more complicated stress state than that applied to the macroscopic bulk) had no effect on the deformation response of each individual grain within a polycrystal aggregate the diffraction anisotropy would closely mimic the single crystal value, but as will be shown in section 5.1 that is not the case.

3.2.1. Single crystal. The single crystal elastic anisotropy, r_E , is defined in the context of uniaxial tension tests on single crystal specimens that have been manufactured with their tension axes aligned with particular crystallographic directions. A directional Young's modulus, $E_{(hkl)}$, may be defined for such an experiment in the $\langle hkl \rangle$ crystallographic direction as in:

$$E_{(hkl)} = \frac{\sigma_{(hkl)}}{\epsilon_{(hkl)}}. \quad (15)$$

Here $\sigma_{(hkl)}$ and $\epsilon_{(hkl)}$ are the normal components of crystal stress and lattice strain, respectively, along the $\langle hkl \rangle$ direction which is the tension axis in the single crystal uniaxial experiment. In face-centered cubic (FCC) materials, $\langle 111 \rangle$ is typically the stiffest direction and $\langle 100 \rangle$ the most compliant; the ratio of the moduli in those two directions gives the greatest anisotropy for the material for the given loading:

$$r_E = \frac{E_{\langle 111 \rangle}}{E_{\langle 100 \rangle}}. \quad (16)$$

The property r_E is defined entirely on the single crystal scale and values for various materials can be found in handbooks. Typical values in metals include approximately 1 in tungsten, 2.1 in iron, and 2.9 in copper; aluminum is reported as having $r_E=1.2$ [22].

3.2.2. Polycrystal. The second manifestation of elastic anisotropy that we consider here is the diffraction anisotropy, r_D , which is the value found from ND experiments on polycrystals and is inherently multiscale in nature. Lattice strains are measured in groups of crystals instead of in single grains. Therefore, $\epsilon_{(hkl)}$ is unavailable to us, and we must instead make use of $\epsilon_{(hkl)}^D$ from (14). Also, since the particular stresses that are present in the individual grains are

unknown, $\sigma_{\langle hkl \rangle}$ is unavailable to us as well. We must instead be satisfied with σ_{macro} , which is the axial component of the macroscopic engineering stress applied to the test specimen. Using these values, we define the diffraction modulus in the $\langle hkl \rangle$ direction, $E_{\langle hkl \rangle}^{\text{D}}$, as:

$$E_{\langle hkl \rangle}^{\text{D}} = \frac{\sigma_{\text{macro}}}{\epsilon_{\langle hkl \rangle}^{\text{D}}}. \quad (17)$$

Further, r_{D} may now be defined as

$$r_{\text{D}} = \frac{E_{\langle 111 \rangle}^{\text{D}}}{E_{\langle 100 \rangle}^{\text{D}}}. \quad (18)$$

From equations (17) and (18) it would appear that r_{D} could also be calculated simply as $\epsilon_{\langle 100 \rangle}^{\text{D}}/\epsilon_{\langle 111 \rangle}^{\text{D}}$ since σ_{macro} appears in both the numerator and the denominator, but in general diffraction measurements of different $\langle hkl \rangle$ s are not made simultaneously. Though the nominal desired load may be identical between measurements, the actual load, and therefore the actual σ_{macro} , may differ and (18) should be used.

Clearly, r_{D} is far from the single crystal property r_{E} . In addition to linking scales between the macroscopic stress and the lattice strains, r_{D} is also a product of averaging responses in groups of largely independent crystals, each of which is subjected to a slightly different micromechanical stress state from its physical neighbors within the aggregate. While the diffraction anisotropy is influenced by the single crystal value, the two are not expected to be equal. Studies have also shown that lattice strains measured after plastic deformation can exhibit different behavior than those measured during purely elastic deformation, further complicating measurement of elastic anisotropy [23–25]. The FE simulations utilized here provide a method of connecting r_{D} to r_{E} . Using an input value r_{E} , the value of r_{D} can be calculated following the method in section 4.2. This gives an indication of what single crystal value may be present when the experimentally measured results are found.

The method of determining r_{D} from experimental data is essentially to take a ratio of slopes, each of which relates a change in macroscopic stress to a change in directional lattice strain. During the ND experiments we collect lattice strains as in (14), which can then be plotted against the scalar value of macroscopic stress at which they are measured. When that process is repeated for each measurement of a specific lattice direction, a plot such as figure 4(a) results. A simple linear regression can then be performed on the data, and the slope of the fit line, as shown in figure 4(b), is identified as $E_{\langle hkl \rangle}^{\text{D}}$. This process is repeated for $\{222\}$ and $\{400\}$ planes, which provide $E_{\langle 111 \rangle}^{\text{D}}$ and $E_{\langle 100 \rangle}^{\text{D}}$, respectively. Taking the ratio of these two values gives r_{D} for the sample.

3.3. Stress distributions

A second aspect of the mechanical response of polycrystals that relates to the interaction of grains under load is the variability of stress within and among the crystals constituting the bulk. The mutual constraints that grains place on each other are affected by a variety of factors, including the degree of mechanical anisotropy, the strength of the crystallographic texture and the geometry of the grains. Thus, the manner in which grains are discretized in a simulation plays a role in the degree of variability in the computed stresses. While isolated grains of the same orientation and shape would exhibit identical responses according to the model, stress variation can stem from the influence of abutting grains. Each unique neighborhood of grains can lead to unique constraints. Locally, stress may be elevated over volumes that experience a strong influence of the constraints. The domains where stress concentrations arise are of interest in assessing where plastic flow initiates and in predicting the location of failure sites.

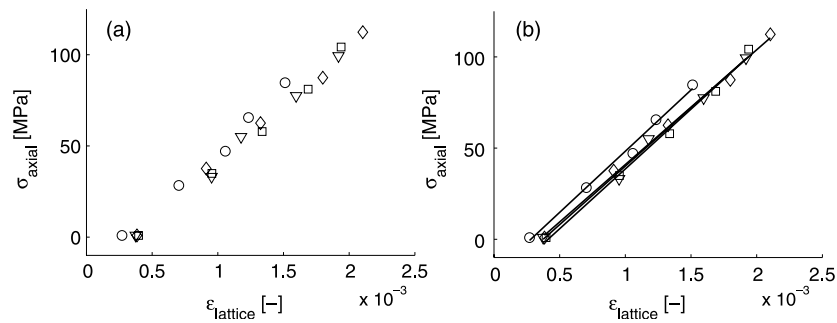


Figure 4. Each measurement of lattice strain in the $(2\ 2\ 2)$ direction in the 2%Mg specimen both (a) without and (b) with linear fits to the data from each unloading episodes. The slopes of the fit lines in (b) are values of $E_{(2\ 2\ 2)}^D$. The different symbols represent separate unloading episodes.

Published literature on this topic reports that variability in the stress exists during loading and following unloading. The most direct evidence is available from x-ray diffraction methods that permit interrogation of individual grains under *in situ* loading, such as the experiments presented in [21]. The standard deviation of the axial component of the lattice strain in copper under tensile loading was examined for twenty crystals sharing the same Bragg condition. The standard deviations of the strain were computed from the peak shifts with changes in load and were on the order of 6% of the average values.

Less direct evidence is available from peak broadening of *in situ* measurements on bulk samples. Broadening occurs from several sources, some related to the instrument and others to the sample, including effects of spatial heterogeneity of the stress and of defects in the microstructure. These are difficult to separate. Examination of broadening during plastic straining of aluminum and stainless steel alloys has been reported in [26]. In that paper, the broadening from stress variations among crystals satisfying one Bragg condition was estimated from simulation and subtracted from the measured overall increase in width. The contribution to peak width from the stress variation was relatively small in comparison with the total change in width which means that using the width changes to estimate stress variability may be prone to error, especially when strain hardening is significant.

The difficulty in experimentally quantifying the spatial distribution of stress over a polycrystal motivates the use of simulation to assist in this task and places a high expectation on the quantitative accuracy of numerical estimates. Again, the sensitivity of the computed responses to the grain discretization is potentially an issue. Intra- and inter-grain variabilities are expected to depend on discretization owing to the differences in the numbers of neighbors with each type of discretization and to the manner in which each grain geometry can be divided by tetrahedral elements.

4. Modelling the experiments

Comparing simulation results for meshes with different grain discretizations must be done for some particular deformation. Whether one of those grain discretizations is preferable to another must be judged on the basis of data that can be extracted from experiments. We use deformations taken from experiments that have been performed on an array of aluminum–magnesium alloys and initialize the simulations to match the global responses. We can then analyze the response of each mesh in terms of elastic moduli and stress distributions to observe any effects of the different meshes used. In the FE simulations, all of the stress

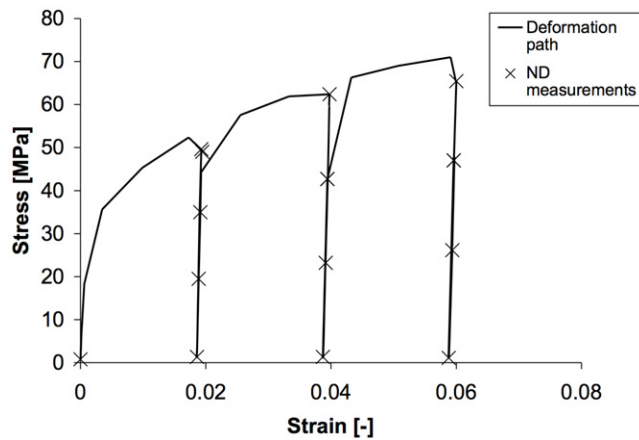


Figure 5. An example of the macroscopic deformation history to which the dogbone specimens are subjected. The somewhat angular appearance of the curve is due to a low sampling rate of load frame measurements. The actual response is smooth. ND measurements are taken at the conditions marked in the figure.

and strain quantities are available at the crystal scale and their resultants over the bulk may be computed. Material properties must be presumed *a priori*, macroscopic deformation is imposed through boundary conditions, and all crystal strains and stresses are calculated during the simulation. The FE formulation itself provides a method of linking between the macroscopic and lattice scales, much as the methods described in section 3 have done.

4.1. Determination of model parameters

The experiments used to initialize the simulations are uniaxial tension on flat dogbone specimens, and are explained in greater detail in [4]. Briefly, a range of aluminum–magnesium alloys (up to Al–8%Mg) were subjected to a deformation history similar to that shown in figure 5. A number of ‘unloading episodes’ are performed during the course of accumulating a total macroscopic strain of less than 10%. During these unloading episodes several ND measurements are made. The experiments focussed on strain variability are described in [21] and consist of measurement of {440} reflections in 20 individual grains in a bulk copper polycrystal measured with high energy XRD. The simulations are not explicitly based on those experiments but the stress distributions found here are compared to those from [21].

Our goal is to uncover any grain discretization dependent effects on the elastic anisotropy and lattice strain variability of the FE simulations. Therefore, we wish to hold as many variables as possible constant between the various simulations. Necessary inputs include: (i) meshes, (ii) boundary conditions and deformation histories, (iii) initial textures and (iv) material properties. The meshes have been described in detail in section 2.2; the origin and generation of each of the remaining inputs is described here.

4.1.1. Loading conditions. The boundary conditions are set to model the uniaxial tension ND experiments. Those experiments were performed at a constant displacement rate of $4.23 \times 10^{-3} \text{ mm s}^{-1}$ (0.01 in min^{-1}) on specimens with gage lengths of 50.8 mm (2 in). Therefore, the approximate initial strain rate is $8.3 \times 10^{-5} \text{ s}^{-1}$. For all the FE meshes, the domain is a cube with tension occurring in the z direction. Symmetry conditions are applied to

the negative x , y and z faces of the mesh to prevent rigid body motions. Free surface boundary conditions are applied to the positive x and y faces, which correspond to the lateral faces of the tension specimen. A constant displacement rate is applied to the positive z face to match the initial strain rate from the experiments.

The deformation history of every experiment followed the same protocol, as shown in figure 5. To recreate that deformation history, certain load setpoints are chosen for each material corresponding to the stress levels at which the unloading episodes initiated and at which the ND measurements were taken. The boundary conditions and deformation histories used do not vary from one mesh to another.

4.1.2. Texture initialization. Bulk texture measurements of both the initial and final conditions were made on a triple-axis spectrometer for specimens of several of the materials [4]. Using these measurements we calculated the orientation distribution functions (ODFs) for those materials. For the measured textures we found that in each material the initial texture is very close to uniform. Therefore, for the materials for which a measured texture is unavailable, we use a texture file that corresponds to a uniform ODF.

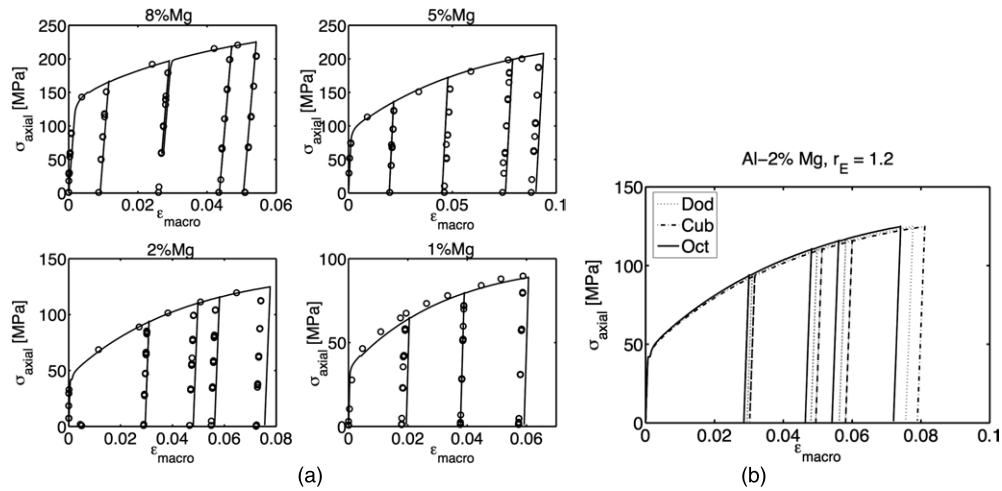
For the simulations each grain must be initialized with a specific orientation. Though no attempt is made to exactly recreate, grain-by-grain, the orientations of the physical specimen, as a whole the orientational texture of the FE domain should match that of the physical domain. Our method of making that match is to create a list of thousands of orientations that, taken together, recreate the ODF. When initializing the element (grain) orientations, we sample randomly from that list. The ODF calculated from the mesh is relatively close to that measured from the physical specimen. This method of texture initialization is independent of the mesh used.

4.1.3. Material properties. The final type of input to consider is the material description. Both the elastic and plastic constitutive parameters must be specified for the simulations. Since we are dealing with cubic materials, there are three independent elastic moduli such as the single crystal elastic moduli commonly referred to as c_{11} , c_{12} and c_{44} [27]. These also can be framed as an average Young's modulus, E , average Poisson's ratio, ν , and the elastic anisotropy, r_E [2]. Young's modulus is measured from the macroscopic stress-strain curves (the average value over the different alloys, 66.5 GPa, is used for all simulations) and Poisson's ratio is kept constant at 0.35. Finally, r_E is varied as a parameter taking the values 1.0, 1.2 and 1.7. For each simulation, therefore, three sets of (c_{11}, c_{12}, c_{44}) are used corresponding to the invariant E and ν and the three values of r_E , as shown in table 2. It is interesting to note that to effect a change on the order of 50% in the single crystal anisotropy it is only necessary to change the individual elastic constants between approximately 8% and 30%.

The parameters associated with slip in (9) and (11) remain to be considered. It is here that the simulations can be said to represent different materials. Some of these parameters were held fixed for all simulations, namely $m = 0.02$ and $\dot{\gamma}_0 = 1.0$, leaving the initial slip system hardening rate h_0 , the initial slip system strength g_0 and the saturation slip system strength g_s yet to be determined. Focussing on each experimental stress-strain curve in turn and using only the dodecahedral mesh, the slip parameters were varied until the macroscopic stress-strain curve from the simulation matched that from the experiment, as seen in figure 6(a). When that match was achieved, those parameters were used for all three meshes, as shown in figure 6(b) for one of the materials, which demonstrates the effect of sharing constitutive parameters across meshes. The value of r_E has very little effect on the macroscopic deformation since the values of E and ν remain constant. Note that the grain shape appears to affect the hardening

Table 2. Elastic material parameters used in FE simulations. All moduli are given in GPa.

r_E	c_{11}	c_{12}	c_{44}
1.0	106.7	57.4	49.2
1.2	103.4	59.1	54.2
1.7	97.3	62.1	63.3

**Figure 6.** Macroscopic stress–strain curves showing the comparison between the experimental data and the three different grain-type meshes. (a) All materials simulated with dodecahedral grains. The solid lines are the simulation results and the marks indicate experimentally measured data. (b) Results from the three mesh types for a single common set of both elastic and plastic constitutive parameters.**Table 3.** Viscoplastic material parameters used in FE simulations.

Material	h_0 (MPa)	g_0 (MPa)	g_s (MPa)
Al–1%Mg	340	17	51
Al–2%Mg	350	21.5	72
Al–5%Mg	400	44	130
Al–8%Mg	425	67	137

rate slightly, which can increase the stress at a given strain. Since the unloading episodes are triggered by a macroscopic stress and not a plastic strain, differences in the ordinate are more significant than differences in the abscissa in figure 6(b). Using the same slip parameters for the different grain shapes appears to be a valid choice. The final choices for plasticity parameters are shown in table 3.

A total of 36 simulations have been performed and analysed here: three sets of elasticity parameters with four sets of plasticity parameters on each of three meshes.

4.2. Calculation of r_D

Finding r_D from the simulation results proceeds in much the same manner as from the experimental data. The first step is to find lattice strains at each stress level, measured in crystals satisfying (13). This is done by indicating those crystals which would contribute to a diffraction

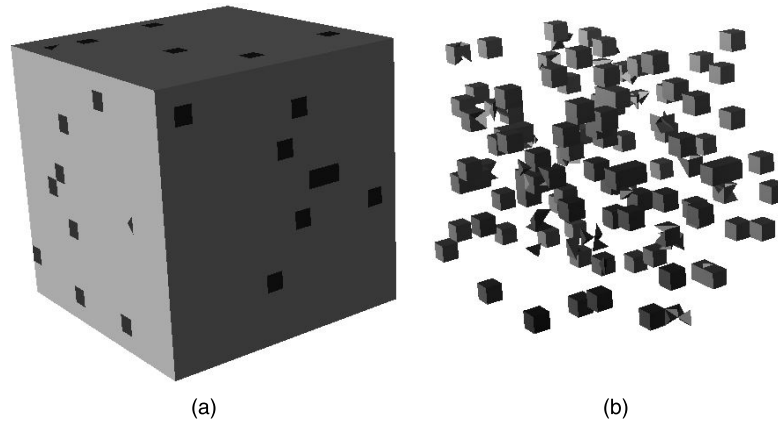


Figure 7. An illustration of elements that contribute to a single measurement during data reduction from the mesh with cubic grains. (a) Complete mesh with contributory elements highlighted. (b) Only those elements which contribute to a diffraction measurement. The elements shown are those that have a misorientation angle less than 5° between their $\{100\}$ planes and the tension axis of the deformation.

measurement, in the same way that the neutron beam and detector illuminate and count certain crystals in any given experimental configuration. For each element in the simulation, a misorientation angle is calculated between the $\{hkl\}$ plane normal and the scattering vector. All elements that have a misorientation angle less than 5° are considered contributory. An example showing elements that have been included in a particular measurement is given in figure 7 for a specific $\{hkl\}$. A single data point on the macroscopic stress versus lattice strain plot is generated by taking the arithmetic mean of the normal lattice strains in the tension direction across all of the included elements:

$$\epsilon_{\langle hkl \rangle}^{\text{sim}} = \frac{1}{l} \sum_{i=1}^l \epsilon_{\langle hkl \rangle}^i, \quad (19)$$

where l is the number of contributory elements, $\epsilon_{\langle hkl \rangle}^i$ is $\epsilon_{\langle hkl \rangle}$ in the i th element and $\epsilon_{\langle hkl \rangle}^{\text{sim}}$ is $\epsilon_{\langle hkl \rangle}^{\text{D}}$ as calculated for the simulation. This is similar to using the center of the Gaussian peak from the neutron diffraction data, as illustrated in figure 3. The stress level is found by taking the load (which is found by integrating the normal stress across all the surface elements that have an applied velocity) and dividing it by the initial cross-sectional area of the domain.

Exactly as for the ND data, the slope of a linear fit to the macroscopic stress versus lattice strain in each direction is defined as $E_{\langle hkl \rangle}^{\text{D}}$ in that direction. The ratio of $E_{(111)}^{\text{D}}$ to $E_{(100)}^{\text{D}}$ provides the value of r_{D} for that simulation.

4.3. Analysis of stress distribution

Two main types of stress distributions are considered: intergranular (among grains) and intragranular (within grains). Intergranular stress variation is calculated by finding the *average value* of σ_{zz} within each grain at any given load level during a simulation, then calculating the standard deviation of those averages throughout the mesh. Intragranular stress variation is calculated by finding the *standard deviation* of σ_{zz} within each grain and averaging those standard deviations over all grains in a mesh. The intergranular stress may be thought of as the

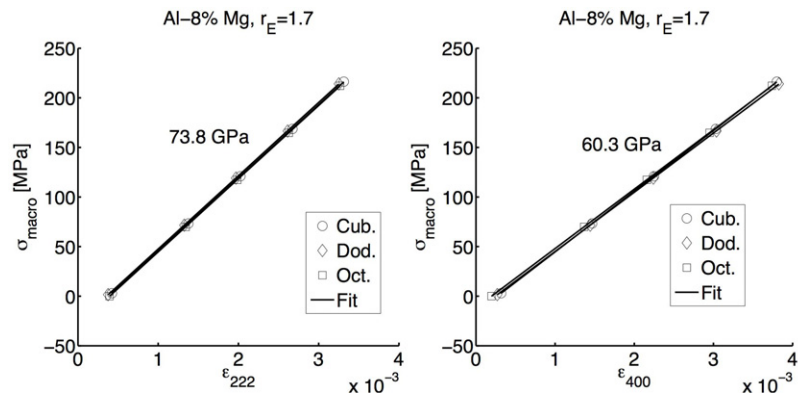


Figure 8. For the simulations of Al-8%Mg with $r_E = 1.7$, the macroscopic axial stress is shown versus the lattice strains. The slope of each line, averaged over the three grain shapes, is shown in each figure.

variation of stress from one grain to another whereas the intragranular stress may be thought of as the amount of variability of stress within each grain.

5. Results

5.1. Diffraction moduli

Following the scheme detailed in section 4.2, values of r_D are determined from each simulation. A typical example of the plots from which $E_{(222)}^D$ and $E_{(400)}^D$ are calculated is shown in figure 8. Any difference in diffraction moduli between the simulations with different grain shapes appears negligible. This means that the diffraction anisotropy appears relatively insensitive to the grain discretizations used here.

In the experiments there is a slight trend of increasing r_D with increasing magnesium content. Using FE simulations, we introduce a method of relating the measurable r_D back to the actual material property r_E . The resulting value of r_D from specified r_E is shown in figure 9 for two sets of plasticity parameters. Slight variations appear between different grain shapes, but figure 8 has demonstrated that those variations are small and not systematic. The significance of this plot is the amount of damping seen between r_E and r_D . A single crystal value of $r_E = 1$ results in apparent isotropy in the diffraction moduli, as expected. If the single crystal properties are isotropic, the particular arrangement of grains should not influence the resulting lattice strains since all directions should be equivalent. As the single crystal anisotropy increases, so too does the diffraction anisotropy. Over the range of r_E studied here, the FE simulations predict an approximate relationship between r_D and r_E as $(\partial r_D / \partial r_E) \approx 0.3$. Averaging over groups of crystals, each of which experiences unique conditions from its neighbors, reduces the apparent elastic anisotropy by up to 30% from the true single crystal property.

It is important to ask whether changes in other material parameters can impact r_D as well. Relationships between r_D and the three slip system parameters that varied between simulations of different materials (h_0 , g_0 and g_s) are shown in figure 10. Clearly the values of these slip system parameters do not affect r_D . Given the material deformation model in use here, the only material parameter that has a significant impact on r_D is r_E .

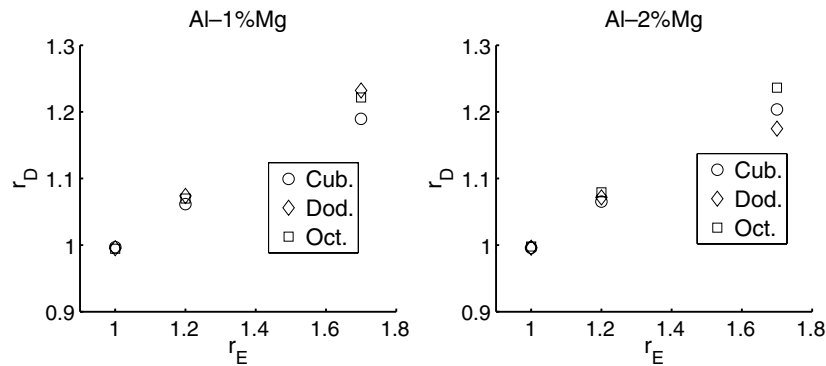


Figure 9. For the simulations of particular materials, r_D is shown versus the input value of r_E for each grain discretization.

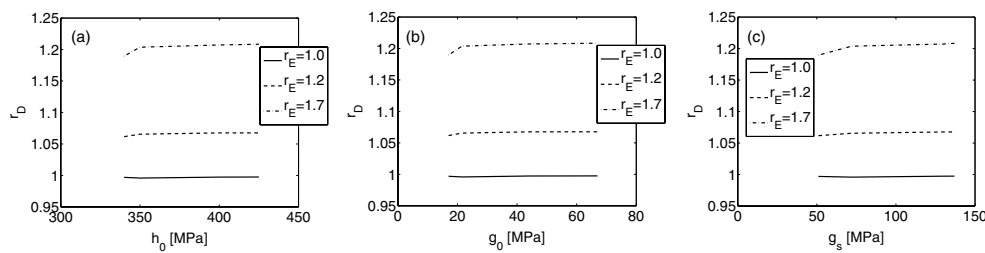


Figure 10. For the simulations with cubic grains, r_D is shown versus the input value of various material parameters.

5.2. Stress distributions

Turning now to stress variations, both among grains (intergranular) and within grains (intragranular), consistent trends with respect to the type of grain discretization emerge. Standard deviations of the axial component of intergranular stresses are shown in figure 11 for one material. Comparable trends are seen in each material modelled. The top and bottom of the last unloading episode are used to generate the data shown. The most variation is seen in the simulations with cubic grains, the least in the octahedral grains. As discussed in section 3.3, typical values found in experiments for variation of strain between different grains satisfying the same diffraction condition are approximately 6% of the average value. It is difficult to make an analogous calculation here since elements that begin the simulation sharing an identical orientation do not always maintain that close orientational relationship through the deformation. In the simulations, a diffraction condition is satisfied (or not) by elements, not by grains, as seen in figure 7(b). Here, we consider all grains in the mesh and see variation in stress of approximately 12%. This higher value is not surprising since portions of the material with different orientations should be expected to experience different stresses.

The trends of intragranular variations are shown in figure 12, and they are opposite to those of intergranular stresses in terms of grain shape dependence: cubic grains show the least variation and octahedral grains the most. The larger number of neighbors experienced by the octahedral grains may generate a greater variety of boundary conditions on a single grain than in the cubic grains. This explains both the larger variation of stress within each grain and the smaller variation of stress between grains for the octahedral shape. If each grain is allowed to

conform to the neighboring crystals on each side, though the variation within a grain may be relatively large, each grain in the mesh will experience that condition; in effect each grain is becoming more like the whole, which can act to diminish differences between different grains. In the cubic grains (with only six neighbors) each grain can act more independently and is less likely to be experiencing a neighborhood similar to other grains, thereby emphasizing differences between grains. One aspect of the differences in grain discretizations whose influence we cannot rule out is the greater number of elements comprising the octahedral grains. Due to their differences in shape it is difficult to mesh each type of grain with identical numbers of elements and thus to remove this unwanted degree of freedom. The larger number of degrees of freedom within the octahedral grains may enhance the effects of having more neighbors.

Looking at the magnitudes of the standard deviations in figures 11 and 12, it is at first somewhat surprising that the amount of stress variation within grains is equal to or greater than the stress variation between different grains. This is most likely due to the averaging of stress within grains that takes place for the intergranular stress calculation. The standard deviation of stress over all elements in the mesh, with no averaging within grains, is shown in figure 13 for the same conditions as figures 11 and 12. There the magnitude is greatest of all, as expected.

In both the intergranular and intragranular stress variations there is a common trend wherein the standard deviations are independent of r_E in the loaded state but highly dependent on r_E in the unloaded state. The stress state is constrained by the plasticity model to lie on the flow surface during plastic flow. Recall that while modelling deformation of each material, the plasticity parameters do not change while r_E does. Therefore, the flow surface is relatively independent of the elasticity parameters. Similar, but not identical, stress states are reached once the material yields and begins to flow. This produces comparable values of standard deviation of the stress distribution. In contrast, unloading from the plastic regime is essentially an elastic event, and changes in stress with unloading are directly dependent on the elastic moduli. Interestingly, the stress changes occurring under higher elastic anisotropy produce a more uniform stress state (lower values of the standard deviation of stresses) than if the elasticity is more isotropic. As can be seen, for the elastically isotropic case of $r_E = 1.0$ there is very little difference between the loaded and unloaded states. This is expected since as the loads are removed all crystals will tend to relax and unload to the same degree, which would give no source for changing the relative stress levels that were established under load. For FCC crystals with $r_E > 1.0$, the crystallographic dependence of the strength and elasticity both show an increase from the $\langle 100 \rangle$ to the $\langle 111 \rangle$ directions, which may allow crystals with high stress to more readily relax upon unloading.

6. Conclusions

Deformation and *in situ* ND of several aluminum alloys has been modelled using elastoviscoplastic FE simulations with meshes formed from grains of different shapes and packing arrangements. The diffraction anisotropy calculated from the simulation results has been compared across meshes and materials. By changing the individual single crystal elastic moduli by less than 30%, the single crystal anisotropy has been changed by over 50%. In doing so, the simulations show a relationship between r_D and r_E of $(\partial r_D / \partial r_E) \approx 0.3$ independent of the grain discretization.

Intergranular and intragranular stress variations are found to depend consistently on the grain shape, with octahedral grains showing the most intragranular and least intergranular variation, and vice versa for cubic grains. The amount of stress variation for all meshes is reasonably consistent with values found in experiments. For all grain shapes, stress variation

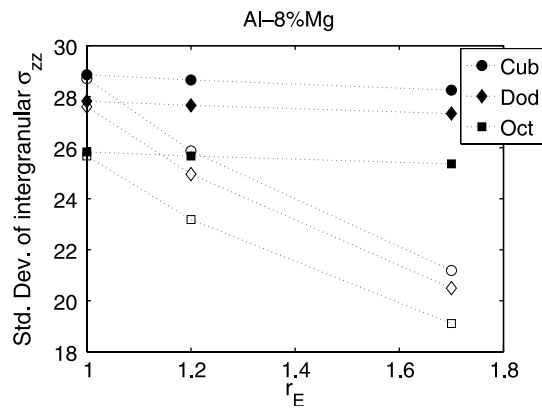


Figure 11. Trends in stress among grains (intergranular) are shown for both loaded (solid markers) and unloaded (empty markers) configurations. For each grain an average stress value is computed, and the standard deviation between those granular averages is shown in units of MPa. The macroscopic stress level in the loaded state is ~ 200 MPa.

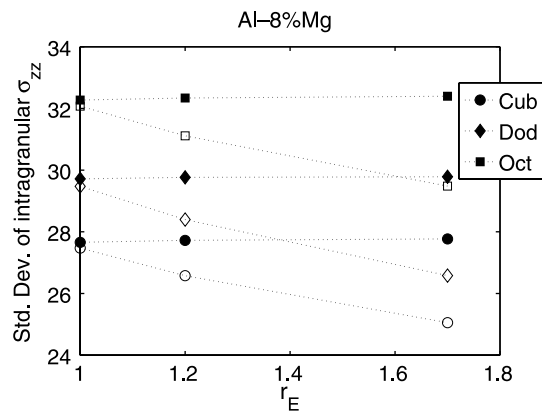


Figure 12. The average standard deviation of the axial component of stress within grains (intragranular) is shown for both loaded (solid markers) and unloaded (empty markers) configurations in units of MPa. The macroscopic stress level in the loaded state is ~ 200 MPa.

is maximal at higher loads and decreases upon unloading. Larger elastic anisotropy causes a larger drop in stress variation with unloading.

When deciding which grain discretization to utilize in FE simulations it is necessary to weigh the relative benefits of different options. Cubic grains, as realized in this study, have fewer degrees of freedom, sharper corners and fewer neighbors than octahedral grains. This allows a greater number of crystals to be modelled with a given allotment of computing resources. If the main interest of the project is something for which a greater number of grains would be a major benefit (for example, texture evolution) this may be a good choice. If, however, capturing trends in stress development and variation is more important, the additional degrees of freedom and more realistic neighborhoods of the octahedral grains may be a better choice.

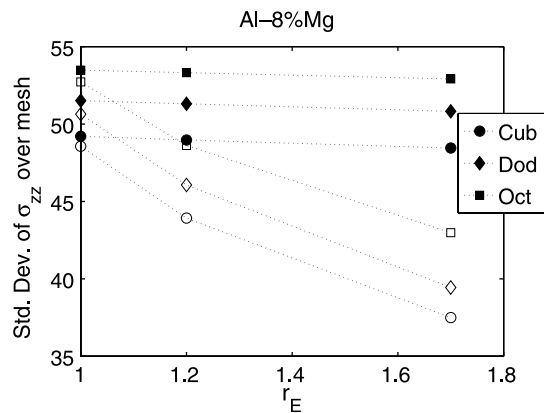


Figure 13. The standard deviation of the axial component of stress over all elements in the mesh is shown for both loaded (solid markers) and unloaded (empty markers) configurations in units of MPa. The macroscopic stress level in the loaded state is ~ 200 MPa.

Acknowledgments

Funding for this project has been provided by the National Science Foundation Graduate Research Fellowship Program and the Office of Naval Research under grant #N00014-05-1-0506. All FE simulations for this project were conducted at the Cornell University Center for Advanced Computing (formerly the Cornell Theory Center (CTC)). Grateful acknowledgment is made to Linda Callahan and Daniel Sverdlik, both formerly of CTC, for assisting with special resource allocation there. Thanks also to Donald Boyce who provided invaluable support and advice with OpenDX figure generation and general data analysis, and Matthew Miller who provided helpful feedback on the manuscript.

References

- [1] Bunge H, Kiewel R, Reinert T and Fritsche L 2000 *J. Mech. Phys. Solids* **48** 29–66
- [2] Dawson P, Boyce D, MacEwen S and Rogge R 2001 *Mater. Sci. Eng. A* **313** 123–44
- [3] Dawson P, Boyce D, MacEwen S and Rogge R 2000 *Metall. Mater. Trans. A* **31** 1543–55
- [4] Ritz H, Dawson P and Rogge R 2008 *J. Neutron Res* at press
- [5] Clausen B and Bourke M 2001 *Metall. Mater. Trans. A* **32** 691–4
- [6] Senechal M 1981 *Math. Mag.* **54** 227–43
- [7] Delannay L, Jacques P and Kalidini S 2006 *Int. J. Plasticity* **22** 1879–98
- [8] Matthies S, Priesmeyer H and Daymond M 2001 *J. Appl. Crystall.* **34** 585–601
- [9] Voigt W 1928 *Lehrbuch Kristallphysik* (Berlin: Teubner)
- [10] Reuss A 1929 *Z. Math. Mech.* **9** 49
- [11] Kroner E 1958 *Z. Phys.* **151** 504–18
- [12] Eshelby J 1961 *Progress In Solid Mechanics* vol II (Amsterdam: North-Holland)
- [13] Bollenrath F, Hauk V and Muller E 1967 *Z. Metall.* **58** 76–82
- [14] Hayakawa M, Imai S and Oka M 1985 *J. Appl. Crystall.* **18** 513–8
- [15] de Wit R 1997 *J. Appl. Crystall.* **30** 510–11
- [16] Gnaupel-Herold T, Brand P C and Prask H J 1998 *J. Appl. Crystall.* **31** 929–35
- [17] Singh A 1998 *J. Appl. Phys.* **83** 7567
- [18] Wenk H, Lonardeli I, Pehl J, Devine J, Prakapenka V, Shen G and Mao H 2004 *Earth Planet. Sci. Lett.* **226** 507–19
- [19] Bragg W 1913 *Proc. Camb. Phil. Soc.* **17** 43–57
- [20] Ice G, Larson B, Tischler J, Liu W and Yang W 2005 *Mater. Sci. Eng. A* **399** 43–8
- [21] Lienert U, Han T S, Almer J, Dawson P, Leffers T, Margulies L, Nielsen S, Poulsen H and Schmidt S 2004 *Acta Mater.* **52** 4461–7

- [22] Hosford W F 1993 *The Mechanics of Crystals and Textured Polycrystals* (New York: Oxford University Press)
- [23] Weidner D J, Li L, Davis M and Chen J 2004 *Geophys. Res. Lett.* **31** L06621
- [24] Merkel S and Miyajima N 2006 *J. Appl. Phys.* **100** 023510
- [25] Merkel S and Yagi T 2006 *J. Phys. Chem. Solids* **67** 2119–31
- [26] Dawson P R, Boyce D E and Rogge R 2005 *Mater. Sci. Eng. A* **399** 13–25
- [27] Nye J F 1967 *Physical Properties of Crystals* (London: Oxford University Press)